Supplementary Information

Supramolecular Quantum Dots as Biodegradable Nano-Probes for Upconversion-Enabled Bioimaging

Fei Zhao, Zhe Li, Lixia Wang, Chuangang Hu, Zhipan Zhang, Chun Li,* and Liangti Qu,**

I. Experimentals.

Materials

Melamine, sulfuric acid (H_2SO_4), potassium permanganate ($KMnO_4$), hydrogen peroxide (H_2O_2) and sodium hydroxide (NaOH) were purchased from Sinopharm Chemical Reagent Co., Ltd. (Shanghai, China). Unless otherwise specified, all reagents were used without further purification.

Preparation of Supramolecular Quantum Dots (SQDs)

The SQDs were prepared through a facile solvothermal reaction. In detail, the graphitic carbon nitride (g-C_3N_4, obtained from thermal condensation of melamine at 500 ºC for 2 h) was treated by concentrated sulfuric acid and $KMnO_4$ to prepare g-C_3N_4 oxide as we previously reported.[S1] The g-C_3N_4 oxide was dissolved in deionized water (DI-water) with a concentration of *ca.* 500 mg/mL. The g-C_3N_4 oxide aqueous solution was ultrasonicated for 30 minutes (100 W, 100 kHz) and the pH was tuned to 8 with NaOH. Then the solution was transferred to a poly(tetrafluoroethylene)-lined autoclave (80 mL) and heated at 160 ºC for 4 h. After cooling to room temperature naturally, the obtained mixture was filtered through a 0.22 μm microporous membrane a limpid filtrate was obtained. The as-obtained filtrate was further dialyzed in a dialysis bag (retained molecular weight: 8500 Da) for 5 h and the water soluble SQDs were obtained with a final yield of *ca.* 35 %. The purified SQDs were finally obtained by freeze drying the resulting solution to remove the water, and then re-dispersed in DI-water for subsequent characterization. The control experiment was performed in the absence of oxidation, where the g-C_3N_4 obtained from thermal condensation (650 ºC for 4 h) of

melamine was dissolved in DI-water and applied for hydrothermal process at 200 ºC for 10 h, and the post-reaction treatment was identical with that of SQDs

Emission Quantum Yield (QY) Measurement of SQDs.

The emission QY of N-GQD aqueous solution was measured on a SPEX flourolog-3 fluorimeter according to established procedure.[S2] The optical densities were measured on UV-vis spectra were obtained on a a 5300 pc spectrophotometer. Quinine sulfate in 0.1 M H_2SO_4 (literature quantum yield 0.54 at 360 nm) was chose as a standard. Absolute values are calculated using the standard reference sample that has a fixed and known fluorescence quantum yield value, according to the following equation:

$$\varphi_x = \varphi_s (A_s/A_x) (I_x/I_s) (\eta^2_x/\eta^2_s)$$

Where φ, I A and η are signifying the quantum yield, integrated emission intensity, optical density and refractive index of solvents, respectively. The subscript "s" indicats the data is collected from standard, and the subscript "x" refers to that of unknown SQDs. In order to minimize re-absorption effects absorbencies in the 10 mm fluorescence cuvette were kept under 0.1 at the excitation wavelength (360 nm).

The absorption cross-section were measured using femtosecond laser pulse of Olympus Fluoview multiphoton microscope (FV1000MPE) (680–1080 nm, 80 MHz, 100 fs) as the light source. All measurements were carried out in air at room temperature. The Rhodamine B in water was chose as a standard. Absorption cross-section was calculated using the standard reference sample that has a fixed and known fluorescence quantum yield value, according to the following equation[S3]:

$$\delta = \delta_{ref} (F/F_{ref}) (\varphi_{ref}/\varphi) (C_{ref}/C)$$

where δ is the absorption cross-section value, C is the concentration of solution, F is the fluorescence integral intensities of the solution emitted at the exciting wavelength, and φ is

the fluorescence quantum yield. A large δ with excitation at 800 nm was measured to be 23,000 GM.

Cell Cultivation and Cytotoxicity Evaluation

Hela cells were cultured in high-glucose modified Eagle's medium supplemented with 10% fetal bovine serum and 1 % penicillin/streptomycin (HDMEM) using a four-chambered Lab-Tek coverglass system (Nalge Nunc) (approximately 5×10^5 in each well). All cells were incubated at 37 °C in a CO_2 incubator until approximately 80 % confluence was reached. The aqueous solution of the SQDs was mixed with the culture medium with the concentration of ca. 60 μg/ml and added to three wells of the glass slide chamber (the fourth well used as a control). After incubation for 2 h, the Hela cells were washed three times with PBS (500 μl each time) kept in PBS for bioimaging. To evaluat cytotoxicity of SQDs, Hela cells were cultured for 24 h in an incubator (37 °C, 5% CO_2), and for another 24 h with SQDs at different concentrations (0, 50, 100, 200, 300, 400, 500 and 600 μg/ml) with DMEM high glucose. Then, 10 μl CCK-8 reagents mixed with 100 μl DMEM high glucose was added to each cell well. After further incubation for 4 h, the optical density (OD) of the mixture was measured at 450 nm. The cell viability was calculated according to the equation of Cell Viability [%] = $(OD_{treated} / OD_{control}) \times 100$ %, where the $OD_{control}$ was obtained in the absence of SQDs, and $OD_{treated}$ obtained in the presence of SQDs. Each experiment was performed four times and the average data was presented.

Characterization

The morphology of the samples was examined by scanning electron microscope (SEM, JSM-7001F), transmission electron microscopy (TEM, JEM-2010 electron microscopy), and atomic force microscopy (AFM, Veeco D3100 atomic force microscope). X-ray photolectron spectroscopy (XPS) data were recorded on an ESCALAB 250 photoelectron spectrometer (ThemoFisher Scientific) with Al Kα (1486.6 eV). X-ray diffraction (XRD) patterns were obtained by using a Netherlands 1,710 diffractometer with a Cu Kα irradiation source (λ

=1.54 Å). The UV-Vis absorption and the photoluminescence (PL) spectra were measured with a 5300pc spectrophotometer and a SPEX flourolog-3 fluorimeter. The imaging of Hela cells was presented by Olympus Fluoview multiphoton microscope (FV1000MPE) with pulses of 100 fs at a repetition rate of 80 MHz as the excited light source.

II. Supplementary Results and Discussion.

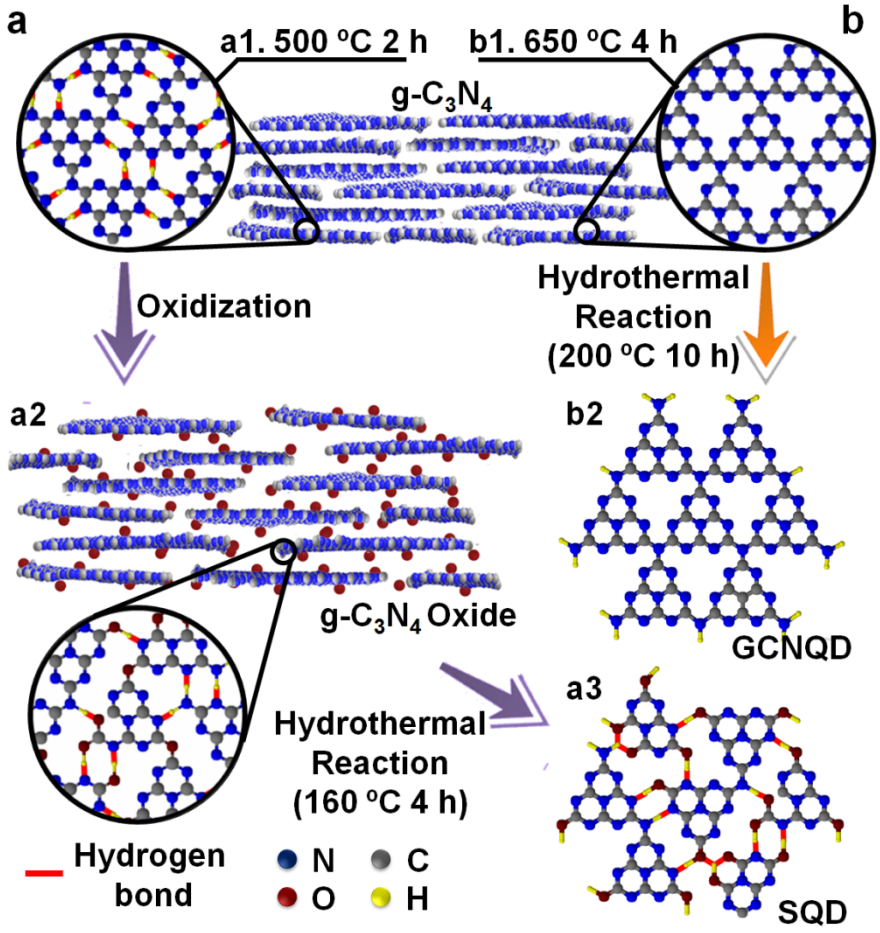

Fig. S1 Schematic illustration of the strategy for the preparation of (a) SQDs and (b) GCNQDs.

Unlike the convenient exfoliation of 2D graphene materials by $KMnO_4$, the oxidative delamination of g-C_3N_4 layers is not particularly effective due to the presence of a large number of interlayer hydrogen-bonds. However, the inner-sheet bonds of g-C_3N_4 became weakened with the oxidation as we reported previously.[S4] As a result, a relatively mild hydrothermal reaction (160 °C for 4 h) was able to foster the cleavage of weak bonds, eventually breaking the g-C_3N_4 oxide sheets into tiny pieces (Fig. S1 a3). In a sharp contrast, the g-C_3N_4 precursors and the reaction conditions for GCNQDs were quite different. The g-

C_3N_4 precursor for GCNQDs was obtained by thermal condensation of melamine at 650 °C for 4 h (Fig. 1 b1), which thus featured a more covalent backbone structure that could only be broken by a more critical hydrothermal treatment at 200 °C for 10 h as shown in Fig. S1 b2. Therefore, due to the presence of the oxidation process in the synthesis of SQDs, the structure and surface properties of SQDs were found to be significantly different to those of GCNQDs

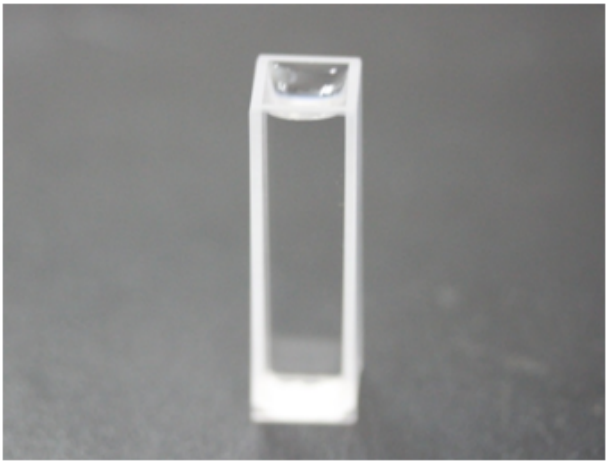

Fig. S2. A photo of SQD aqueous solution

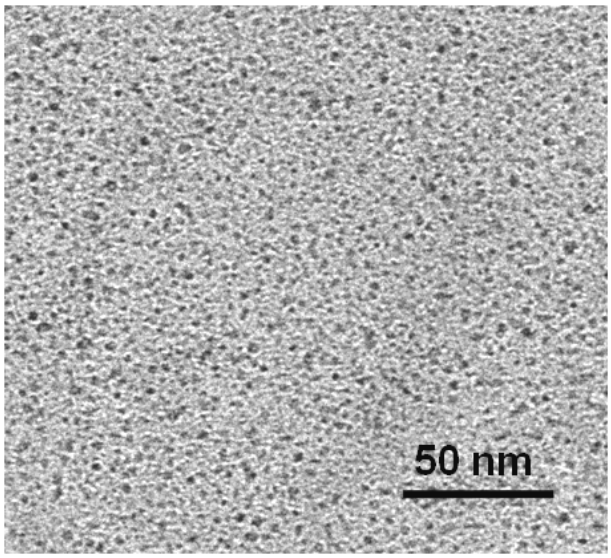

Fig. S3.TEM images of the as-prepared SQDs.

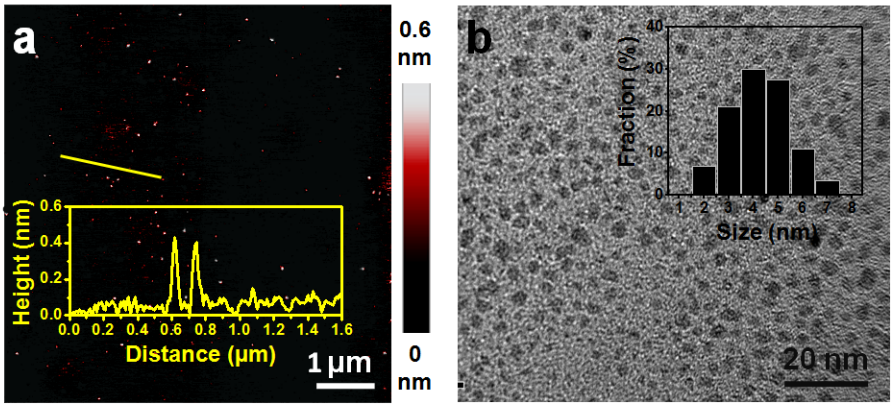

Fig. S4. (a) AFM image of the GCNQDs on a SiO_2 substrate with the height profile along the yellow line; (b) TEM image of the as-prepared GCNQDs with the size distribution.

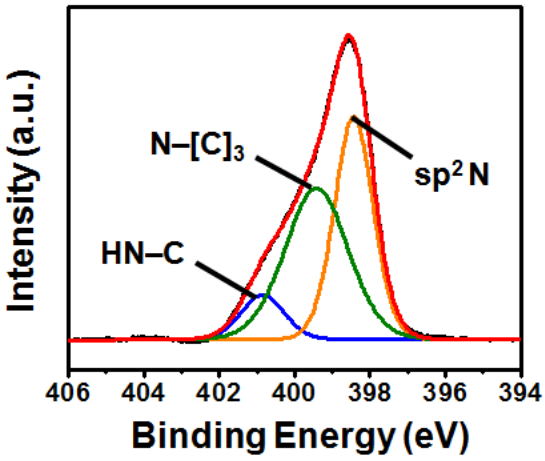

Fig. S5. High resolution N 1s spectrum of SQDs fitted to three energy components centered at around 398.5, 399.5 and 400.9 eV, which can be attributed to sp^2 hybridized nitrogen involved in triazine rings, sp^3-hybridized bridging nitrogen ($N–[C]_3$) and amino functional groups with a hydrogen atom (C–NH), respectively.

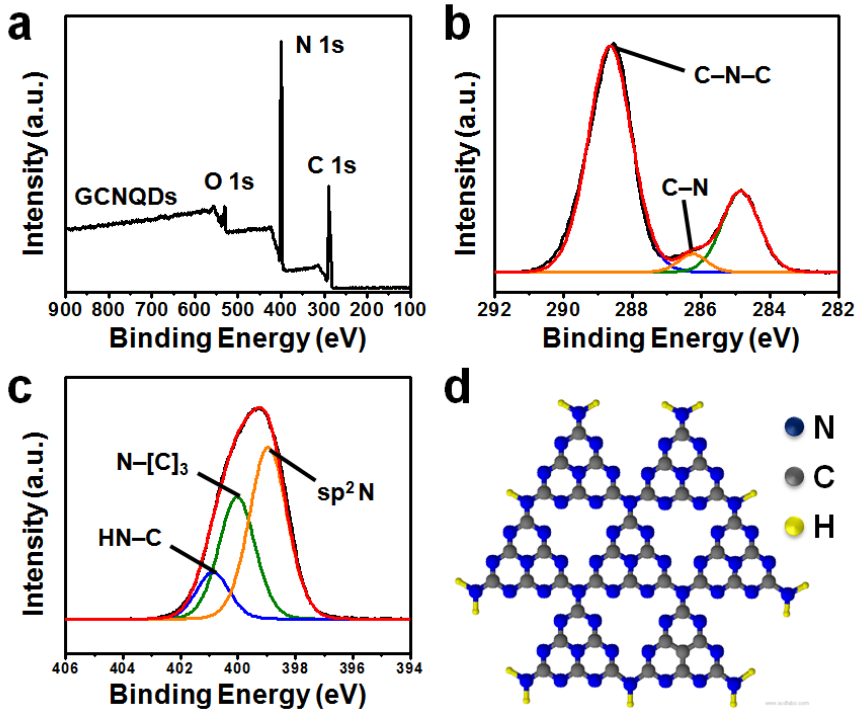

Fig. S6. (a) XPS spectra of the as-produced GCNQDs; (b, c) high resolution O 1s (b) and C 1s (c) peaks of GCNQDs; (d) possible schematic structure of GCNQDs.

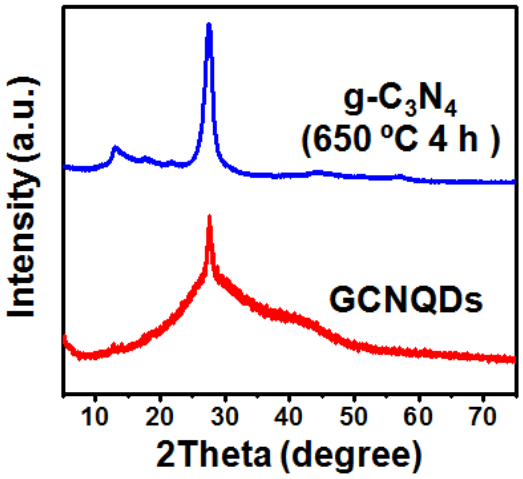

Fig. S7. XRD patterns of g-C_3N_4 prepared by thermal condensation at 650 ºC for 4 h (blue) and GCNQDs (red).

The blue curves in Fig. S7 presented two typical peaks, suggesting that the g-C_3N_4 in current work basically have the same structure as the previously reported g-C_3N_4 with differnt preparation condition.[S5] The corresponding peak becomes less pronounced in GCNQDs, which is mainly caused by the decreased planar size of the tri-s-triazine assembly. With respect to the parent g-C_3N_4, the peak originated from the periodic stacking of layered structures remained distinct in GCNQDs at *ca.* 27.3 °, indicating that the QDs inherited the layered structrure from their precursor.

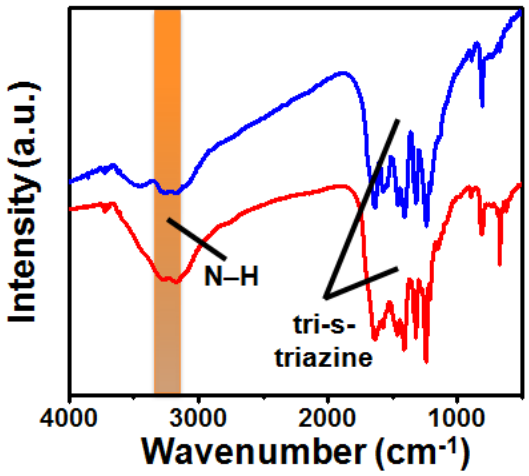

Fig. S8. FTIR spectra of g-C_3N_4 prepared by thermal condensation at 650 ºC for 4 h (blue) and GCNQDs (red).

As shown in Fig. S8, generally, the sharp peak at around 810 cm^{-1} is originated from tri-s-triazine ring system.[S6] The peaks in the region from 1000 to 1800 cm^{-1} are attributed to the trigonal C–N(–C)–C and bridging C–NH–C units, and the broad peaks between 3000 and 3400 cm^{-1} are contributed by N–H stretching.[S6] These evidences proved that all of the tested samples are constructed by tri-s-triazine ring system. However, there are some structural differences among them. For example, comparing the blue curves in Fig. 1 h and Fig. S8, a shift of the N–H stretching peaks can be clearly observed, which is contributed by hydrogen-bonding interactions, indicating a tri-s-triazine ring system cohered with a large number of hydrogen-bonds. A similar phenomenon was also observed in the comparison of the red curves, suggesting the presence of hydrogen-bonds in SQDs. Additionally, the peaks originating from C–N(–C)–C and C–NH–C in SQDs become less pronounced, implying that the bridging N atoms were replaced consisting with the schematic structures in Fig. S1. Moreover, as demonstrated in XPS analysis, the new peaks locating at 3480 and 1760 cm^{-1} are caused by the oxygen-containing groups, verifying the schematic structure of SQDs as shown in Fig. S1.

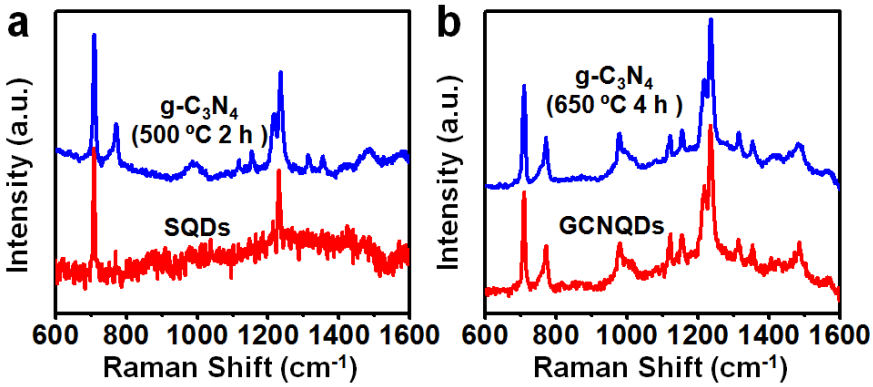

Fig. S9. Raman spectra of SQDs (a, red), GCNQDs (b, red), g-C_3N_4 prepared by thermal condensation at 500 ºC for 4 h (a, blue) and 650 ºC for 2 h (b, blue).

As reported in other literatures,[S7] while the peaks locating at 700 and 1250 cm^{-1} (Fig. S9 a, red curve) come from in-planar bending and stretching vibrations of melem-like structure (describing as tri-s-triazine in the current work), corroborating that the SQDs retained the tri-s-triazine ring system in supramolecular structure as shown in Fig. S1 a3, whereas the GCNQDs have similar C–N planar structure with its parent g-C_3N_4 (Fig. S9 b).

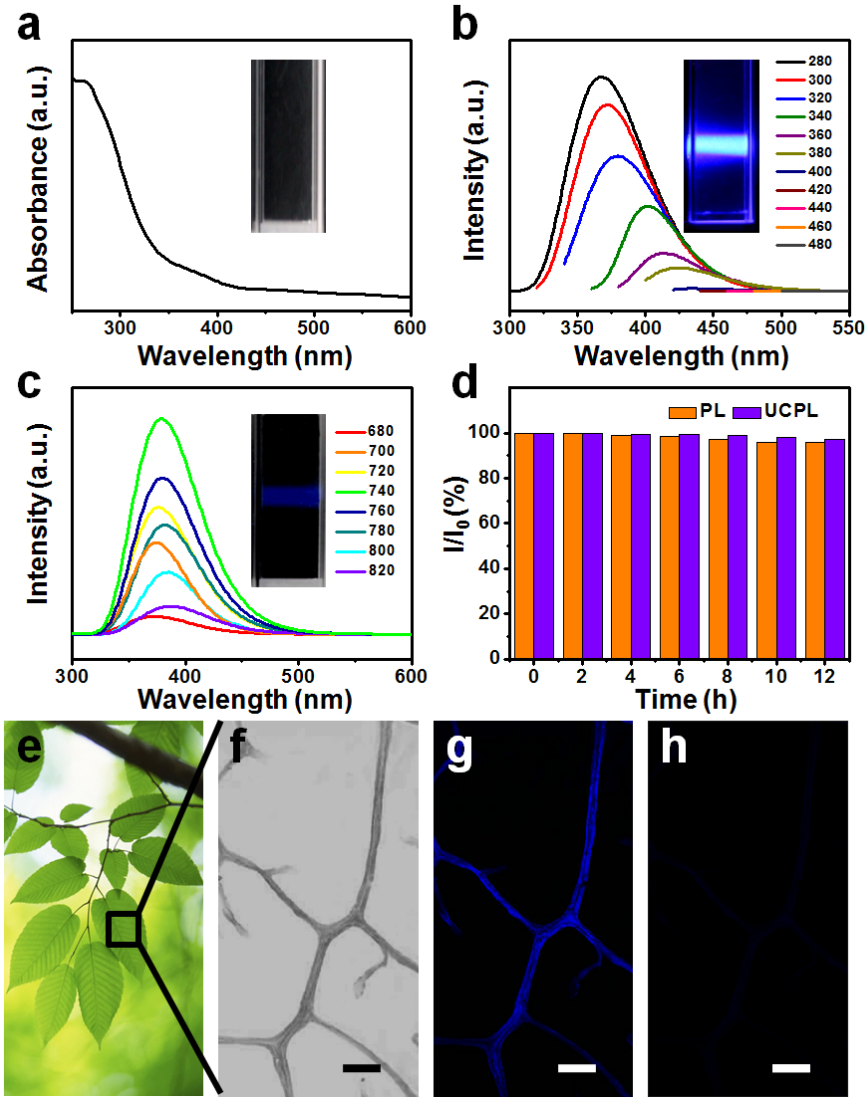

Fig. S10 (a, b, c) UV-vis absorption, PL spectra and UCPL spectra of SQDs in water, inset: photos of the SQD solution in water, with 280 nm and 800 nm exciting light, respectively; (d) Dependence of PL and UCPL intensity on UV-light illumination time for SQDs; (e) Digital photo of leaves; (f, g, h) Bright-field, fluorescent and upconverted fluorescent images of leaf veins stained with SQDs; Scale bars: 50 μm.

The UV–vis absorption spectrum of SQDs shows an absorption band centered at *ca.* 274 nm (Fig. S10 a), standing for a *ca.* 100 nm blue shift with respect to that of the original g-C_3N_4. Under the illumination of a 280-nm UV lamp (20 W), the aqueous dispersion of SQDs (Fig. S10 a, inset) emits an intensive blue luminescence (Fig. S10 b, inset) with a quantum yield of

ca. 27.6 % that is in different to the green luminescence of the g-C_3N_4 precursor, indicating a different band structure of SQDs to that of the g-C_3N_4. Generally, the band gap of g-C_3N_4 is reduced through dense stacking of the sp^2 aromatic clusters due to the formation of strong overlap in the orbital, however, as SQDs are only single-layered, the stacking-induced narrowing of band gap no longer exists. Furthermore, it has been reported that the g-C_3N_4 contains a number of sp^2 C-N clusters formed by tri-s-triazine (melem) units, and the current hydrothermal exfoliation of the g-C_3N_4 could presumably form SQDs with much smaller sp^2 clusters, opening up a larger optical band gap and leading to a hypsochromic shift in photoluminescence (PL). Meanwhile, the emissions of SQDs are excitation-dependent (Fig. S10 b), demonstrating a monotonic decrease in energy and intensity with the increasing excitation wavelength and implying the PL properties of SQDs originate from the quantum confinement effects rather than exclusively from the intrinsic property of g-C_3N_4. In comparison, while GCNQDs are similar in size to SQDs, they exhibit excitation-dependent PL emissions with a *ca.* 30 nm red shift with respect to those of the SQDs under the same excitation wavelengths, suggesting that the exciton localization induced by the supramolecular structure plays an important role in the fluorescence process of SQDs.[S8,S9]

Intriguingly, the as-synthesized SQDs possess upconversion PL (UCPL, Fig. S10 c) properties. As shown in Fig. S10 c inset, SQDs exhibit blue-colored UCPL under the excitation of 800 nm light with an absorption cross-section value of *ca*. 23,000 GM, which is comparable with that of triplet−triplet annihilation upconversion and slightly lower than that of rare-earth upconversion nanoparticles.[S10] The peak position of UCPL is found to remain almost unchanged at *ca.* 380 nm when the excitation wavelength changes from 680 to 820 nm, similar to the case of reported inorganic semiconductor QDs that have fixed UCPL peak positions independent of excitation wavelength.[S11,S12] It is worth noting that during the UCPL measurement, the cutoff filters were put in the excitation channel between the excitation source and the sample in order to eliminate the diffraction light from light source

and therefore exclude any misleading emission excited by second-order diffraction light of wavelength λ/2 that coexists in the selected light (first-order) of wavelength λ from the monochromators of the spectrofluorimeter. In the meantime, the UCPL cannot be observed in the control sample of GCNQDs, suggesting that the UCPL of SQDs must be related to their supramolecular structure and/or unique surface properties that could be presumably attributed to an excited state absorption schematically illustrated in Fig. S11. Both PL and UCPL of SQDs are stable, with no obvious change in the intensity over 12 hours (Fig. S10 d), qualifying SQDs as an excellent candidate for NIR exited bioimaging that is a noninvasive and traceless method to observe deep inside various cells of living organisms. As an initial attempt, the solution of SQDs was utilized to stain the veins of holly leaves (Fig. S10 e) for a NIR excited imaging. When the root of the leaf, which had been pre-dehydrated by freeze drying, was soaked in SQDs solution, SQDs were taken into the leaf along its veins by capillary force. After the ambient drying, the fluorescent imaging of the veins are shown as Fig. S10 f to h. The cytoderm of veins absorbs near ultraviolet light (405 nm) but are nearly transparent to NIR light (800 nm), thus the NIR excited imaging in Fig. S10 g renders an image with far better resolutions than that carried out under 405 nm (Fig. S10 h).

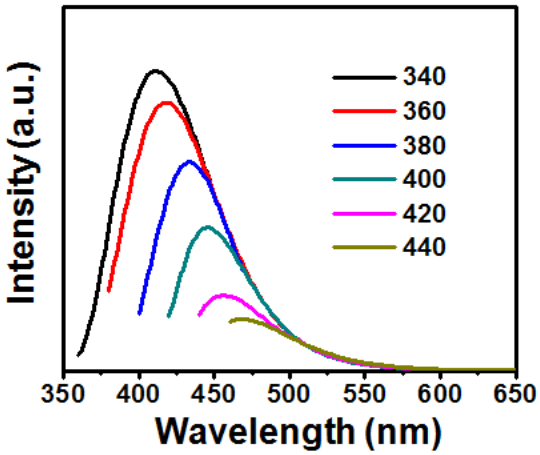

Fig. S11. PL spectra of GCNQDs with 340 to 440 nm exciting light.

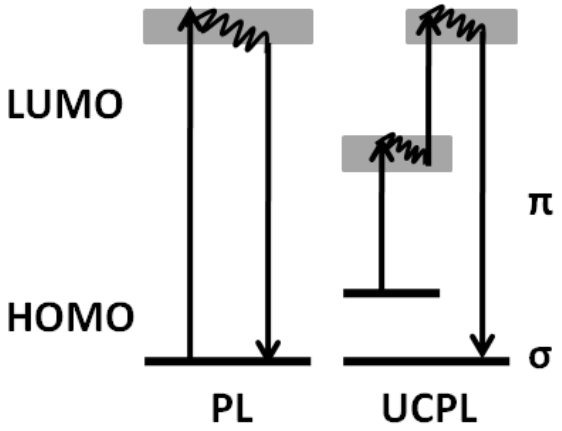

Fig. S12. Schematic of PL and UCPL of SQDs.

Similar to the nano-materials with π-conjugated electronic structure, the fluorescence of SQDs may originate from the π−π* charge-transfer transition of the tri-s-triazine ring structure. Furthermore, as the strong electron donating bridging N (equivalent to dimethylamino group) was replaced by electron accepting O, the large π-conjugated system was separated into small π-conjugated domains with different size, and hence the excited level was splitted.[S13] More importantly, the supramolecular cohering of π-conjugated domains can facilitate the charge transfer between the splitted excited level of π-conjugated domains,[S14] which enabled the excited state absorption induced UCPL. Additionally, the lone pair (LP) electrons from the N of tri-s-triazine rings, which were located in the sp^2 C−N p valence band instead of hybridizing with the carbon,[S15] were easily excited to the aromatic rings to form the p−π conjugation, inhibiting the irradiative recombination on π orbit. As a result, the recombination of excitons was proceed by irradiative transition from excited level to LP state, indicating that the wavelength (λ) of UCPL might be smaller than λ/2 of exciting light.

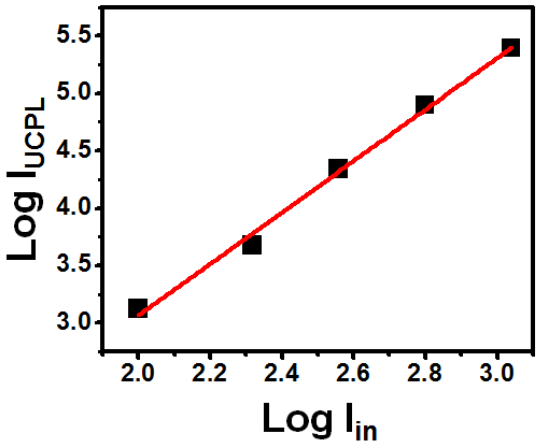

Fig. S13. Quadratic log-linear relationship between the upconversion luminescence intensity of SQDs and the incident laser power. The slope of power-dependent fluorescence intensity as a function of input laser power was *ca*. 2.06, suggesting an two-photon excitation enabled UCPL.

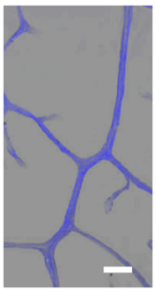

Fig. S14. Merged image of Fig. S10 f and g, showing the uniform distribution of SQDs in veins and suggesting their potential application of deep-tissue imaging. Scale bars: 50 μm.

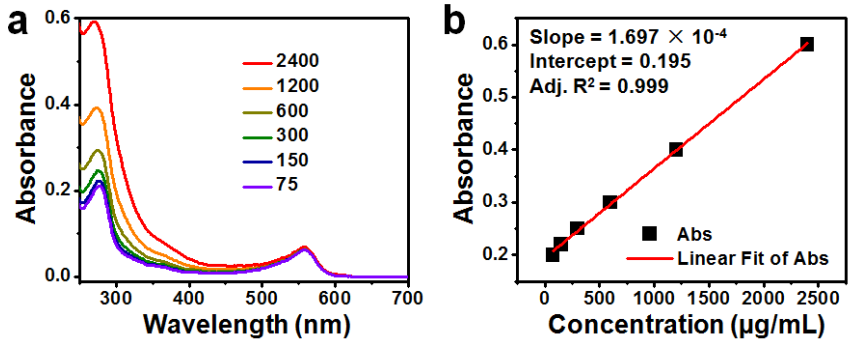

Fig. S15. (a) UV-vis spectra of SQDs in as-inactivated cells solution with concentrations of 2400, 1200, 600, 300, 150 and 75 μg mL^{-1}; (b) A linear relationship between absorbance at 274 nm and the corresponding concentration of SQDs. The SQDs exhibited conspicuous absorbing bands in the solution due to the presence of C-N plane structures and the absorbance of the extraction solutions of as-inactivated cells gradually decreased with the increasing incubation time.

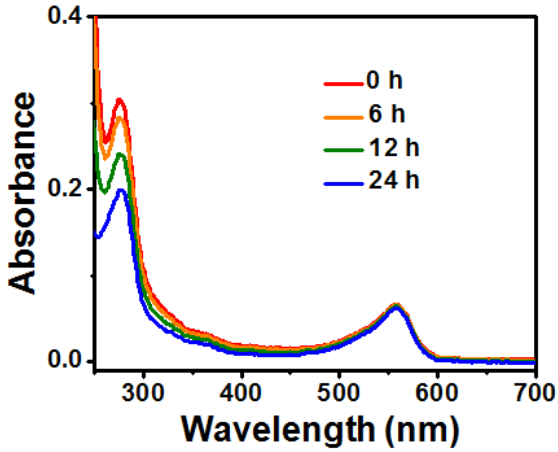

Fig. S16. UV-vis spectra of result solutions obtained from coincubation of Hela cells with SQDs for 0, 6, 12 and 24 h.

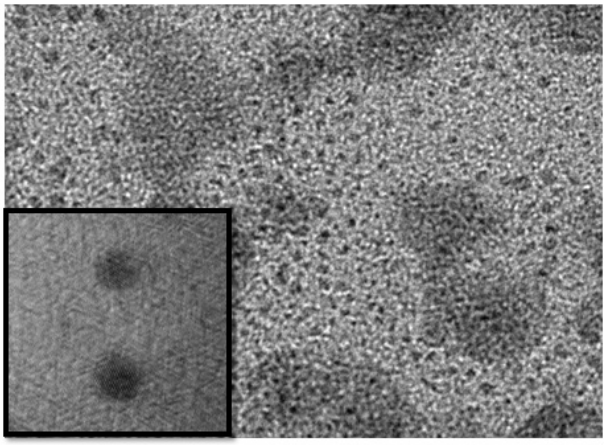

Fig. S17. TEM image of SQDs incubated in the culture medium after 24 h, confirming SQDs cannot be degraded simply by the cuture medium. Inset: high resolution image of SQDs.

Reference to the supplementary information

S1. F. Zhao, H. Cheng, Y. Hu, L. Song, Z. Zhang, L. Jiang, L. Qu, Sci. Rep. 2014, 4, 5882.

S2. J. R. Lakowicz, *Principles of Fluorescence Spectroscopy*, 2nd Ed, Kluwer Academic/Plenum Publishers, New York, 1999, pp. 37.

S3. X. Zhang, H. Wang, H. Wang, Q. Zhang, J. Xie, Y. Tian, J. Wang, Y. Xie, Adv. Mater.2014, 26, 4438-4443.

S4. P. Niu, L. Zhang, G. Liu, H. M. Cheng, *Adv. Funct. Mater.* 2012, **22**, 4763-4770.

S5. X. Wang, K. Maeda, A. Thomas, K. Takanabe, G. Xin, J. M. Carlsson, K. Domen, M. Antonietti, *Nat. Mater.* 2008, **8**, 76-80.

S6. X. Zhang, X. Xie, H. Wang, J. Zhang, B. Pan, Y. Xie, *J. Am. Chem. Soc.* 2012, **135**, 18-21.

S7. L. van Dijk, P. A. Bobbert, F. C. Spano, *J. Phys. Chem. B* 2009, **114**, 817-825.

S8. J. Li, B. Shen, Z. Hong, B. Lin, B. Gao, Y. Chen, *Chem. Commun.* 2012, **48**, 12017-12019.

S9. H. Li, X. He, Z. Kang, H. Huang, Y. Liu, J. Liu, S. Lian, C. H. A. Tsang, X. Yang, S. T. Lee, *Angew. Chem. Int. Ed.* 2010, **49**, 4430-4434.

S10. G. Chen, H. Qiu, P. N. Prasad, X. Chen, *Chem. Rev.* 2014, **114** 5161-5214

S11. L. M. Maestro, E. M. Rodríguez, F. S. Rodríguez, M. I. d. la Cruz, A. Juarranz, R. Naccache, F. Vetrone, D. Jaque, J. A. Capobianco, J. G. Solé, *Nano Lett.* 2010, **10**, 5109-5115.

S12. S. Zhuo, M. Shao, S. T. Lee, *ACS Nano* 2012, **6**, 1059-1064.

S13. C. Xu, W. W. Webb, *JOSA B* 1996, **13**, 481-491.

S14. N. Hirata, J. J. Lagref, E. J. Palomares, J. R. Durrant, M. K. Nazeeruddin, M. Gratzel, D. J. Di Censo *Eur. Chem. A* 2004, **10**, 595-602.

S15. G. Fanchini, A. Tagliaferro, N. Conway, C. Godet, *Phys. Rev. B* 2002, **66**, 195415.